ACS Photonics

pubs.acs.org/journal/apchd5

Article

Ultrahigh Visible-Transparency, Submicrometer, and Polymer-Free Radiative Cooling Meta-Glass Coating for Building Energy Saving

Shilv Yu,[#] Jae-Seon Yu,[#] Zihe Chen, Qinghe Li, Zhaochen Wang, Xiaobing Luo, Sun-Kyung Kim,* and Run Hu*

Cite This: https://doi.org/10.1021/acsphotonics.4c00981

Read Online

ACCESS | Metrics & More | Article Recommendations | Supporting Information

ABSTRACT: Glass windows are the most energy-inefficient part of buildings, which triggers the ongoing chasing of energy-efficient transparent radiative cooling (TRC) metamaterials on glasses that simultaneously maintain high visible (VIS) transparency, block near-infrared (NIR) solar radiation, and emit thermal energy through the atmosphere window (AW). However, the stringent multispectral regulation remains challenging since it involves with huge parameter spaces and significant interactions among different bands. Additionally, most TRC metamaterials require a top ∼50 μm polymer for high emissivity in the AW, which will reduce the VIS transparency and suffer from aging issue. Here, we employ the deep reinforcement learning (DRL) method, leveraging its robust material screening and structure optimization capabilities, to design a five-layer submicrometer dielectric multilayer, composed of two stacked materials, as polymer-free TRC metamaterial on glass or meta-glass for short. Utilizing a plain glass substrate with high emission in the AW, our meta-glass demonstrates an ultrahigh angular-independent (<60°) VIS transmissivity against the state-of-the-art, i.e., 86% (92.7% in theory), with ∼48% NIR reflectivity and ∼89% AW emissivity in experiment. In outdoor experiments at ambient temperatures of ∼10 and ∼20 °C, with solar irradiances reaching around 780 and 850 W/m^2, our meta-glass achieves a floor temperature reduction of 8.9 and 12.7 °C, respectively, compared to uncoated glass. Furthermore, we achieved customization of meta-glasses with varying transparency levels while maintaining high NIR reflectance by DRL. Our meta-glass exhibits an extraordinary building energy saving potential in most climate zones. This work provides a valuable reference for the advancement of TRC and the design of multispectral metamaterials.

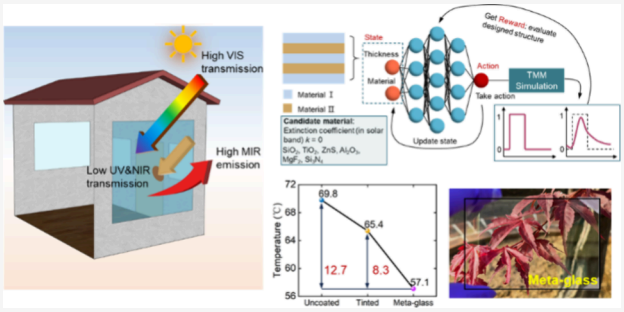

KEYWORDS: *radiative cooling meta-glass, ultrahigh VIS transparency, energy saving, deep reinforcement learning, dielectric multilayer, metamaterial*

INTRODUCTION

Energy-efficient building is one of the important ways to pursuing the carbon neutrality for the whole human society. The heating, ventilation, and air-conditioning (HVAC) systems contribute to nearly 40% of the energy consumption of buildings, especially for the increasing demand of space cooling and heating in buildings for the diverse personal thermal comfort requirements, which in turn exacerbates the carbon emissions and environmental problems such as global warming.[1,2] Moreover, glass facades have been popular in buildings for aesthetic purposes, while glass windows are the least energy-efficient part of buildings, especially for skyscrapers, losing nearly 50% of the energy, as they indiscriminately transmit all incoming solar energy and thus seriously exacerbate space cooling energy consumption.[3,4] It is therefore urgent to develop low-carbon or zero-carbon technologies to reduce the energy consumption of buildings. Fortunately, passive radiative cooling (PRC) provides a feasible solution, which establishes a passive, continuous, and efficient heat transfer channel between the buildings and 3 K outer space through the atmosphere window of 8−13 μm while reflecting solar radiation to decrease the solar absorption as much as possible to achieve subambient cooling temperature.[5−7] Owing to the passive and zero-energy consumption cooling mode, PRC has attracted considerable research attention and development, rendering it the most promising passive cooling technology with many emerging forms, such as photonic crystals, particle-based polymers, fibers and textiles, and sintered ceramics.[8−17] However, most of these PRC materials cannot be directly applied on building windows, since they are usually in white color to reflect the solar light as much as possible to maximize the cooling performance. As a

Received: May 29, 2024
Revised: June 25, 2024
Accepted: June 26, 2024

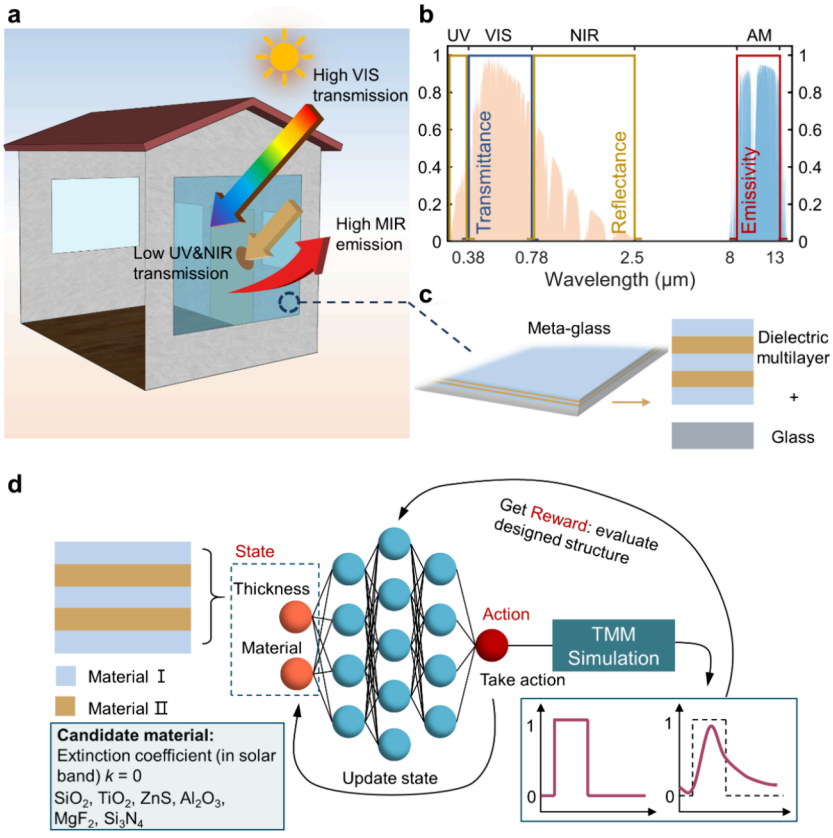

Figure 1. Concept of meta-glass and schematic for the DRL framework. (a) Meta-glass as window materials for building energy conservation. High VIS transmittance, low NIR transmittance, and high MIR emission are simultaneously required for visual transparency, blocking solar heating and dissipating heat. (b) Ideal spectrum of TRC. The orange shade presents the AM 1.5 solar spectrum. The blue shade presents the atmosphere window. (c) Structural schematic of the meta-glass. The top DM is utilized for solar spectral modulation and glass substrate is to ensure high MIR emission. (d) Schematic for the DRL framework. The two materials and five thicknesses of DM are accepted by DQN. DQN outputs an action for updating the structure of DM. TMM is adopted for DM spectrum simulation. Reward function guides the optimization direction. Six candidate materials with extinction coefficient of near zero in solar band are prepared for DQN to chosen for DM.

result, glass with transparent radiative cooling (TRC), or meta-glass for short hereinafter, which allows the transmission of visible light while maintaining substantial PRC performance, has recently attracted increasing attention.[18−21]

In order to enable daytime illumination and PRC concurrently, meta-glass is required to have high transmittance in VIS wavelengths (0.38−0.78 μm) to ensure efficient transmission of light, high reflectivity in the ultraviolet (UV) (0.3−0.38 μm) and NIR bands (0.78−2.5 μm) to block solar radiation to prevent unwanted heating, and high emissivity in the mid-infrared (MIR) wavelength to radiate heat to outer space through the AW (Figure 1a,b). To achieve such stringent wavelength selectivity, the prevalent strategy is to develop a VIS transparent NIR reflector and superimpose a transparent MIR emission layer. The former is to regulate the optical properties of meta-glass in the solar band (0.3−2.5 μm), and the latter is to form a high MIR emissivity. Extensive previous effort has been devoted to only developing the VIS transparent NIR reflectors, as the transparent emission layer can be easily implemented via polymers, like polydimethylsiloxane (PDMS) and poly(methyl methacrylate) (PMMA). With the aid of nanophotonics and metamaterials, VIS transparent NIR reflector can be achieved by (i) dielectric/metal/dielectric (DMD) structures, such as SiO_2/Ag/SiO_2,[22] TiO_2/Ag/TiO_2,[23] and ZnO/Ag/ZnO,[24] (ii) transparent doped semiconductor-based structures, such as indium tin oxide (ITO)[25,26] and fluorine-doped tin oxide (FTO),[27,28] and (iii) dielectric multilayer (DM) structures, such as SiO_2/TiO_2, Si/SiO_2,[29−32] etc. However, most of these designs still rely on conventional empirical methods and manual parameter tuning optimization, leading to low design efficiency and barely satisfactory performance, particularly the VIS transparency. Additionally, this stacking strategy heavily focuses on the bottom NIR reflector, disregarding the impact of the polymer on VIS transparency. Actually, their VIS transparency is not as good as common glass, some even displaying noticeable color variations. We hold the view that VIS transparency should be equally or even more important than cooling performance in assessing meta-glass, as it is the foremost requirement of window glass and directly influences human visual perception. People will not tolerate the windows of their home or office are not sufficiently transparent, or even colored, which not only leads to inadequate daytime illumination and poor visibility to the exterior but may also be negative to their psychology and even physiology.[33] It is worth noting that the specialized use of colored glass is outside the scope of this study and could be further investigated. Furthermore, if the front windshield of an automobile lacks of enough VIS transparency, it may pose some driving safety concerns.

However, achieving extremely high VIS transparency in DMD structures is challenging unless the thickness of metal (such as Ag) is accurately controlled to be thin enough, which, in return, results in higher fabrication accuracy requirement. In addition,

https://doi.org/10.1021/acsphotonics.4c00981
ACS Photonics XXXX, XXX, XXX−XXX

DMD structures inevitably exhibit high reflection in the whole IR band, which leads to the necessity of stacking a polymer layer to achieve TRC. In fact, the polymer must be thick enough (~80 μm) to exhibit high MIR emission (the thickness dependence is discussed in Figure S6), which further reduces the VIS transparency of the entire TRC, typically ~60%. Plain glass, as the commonly used window glass and substrate material for meta-glass, already exhibits high MIR emissivity (~86%).[34] Consequently, the introduction of polymer also increases the complexity of the fabrication process, as the fabrication process of polymer layers is incompatible with DMD layers, and micrometer-scale thickness coatings lead to poor economic viability. In addition, polymers suffer from the aging and reliability problem under long-term direct sunlight.[35] ITO-based TRC glass also depends on polymer materials to support high MIR emission and exhibits suboptimal VIS transparency (~80%) and NIR reflection (~55%).[25] By contrast, DM offers a relatively higher flexible capability for wavelength selectivity characteristics, including the VIS, NIR, and MIR bands. For example, Zhu et al. proposed a stacked DM structure of SiO_2 and TiO_2 to achieve considerable VIS transmittance (~72%) and NIR reflectance (~80%).[31] Nonetheless, the use of up to 30 nanoscale multilayers nearly disables the practicality. Kim et al. employed quantum annealing method to optimize a microscale DM-based TRC glass with atop the PDMS layer, whose VIS transmittance and NIR reflectance reaches ~75 and ~60%, respectively.[29] They employed four different materials for the DM-based TRC glass, and the increased different material interfaces may be vulnerable to thermal and mechanical stresses. More importantly, the nonuniform VIS transmittance of their design causes an obvious color disparity.

In this work, we employ a deep reinforcement learning (DRL) framework for efficient material selection and structure optimization of a five-layered submicrometer DM consisting of two stacked materials (Figure 1c). Combined with a plain glass substrate, a polymer-free meta-glass demonstrates a ultrahigh VIS transmittance of 86% (~92.7% for simulation), along with considerable NIR reflectance (~48%) and AW emissivity (~89%) experimentally. In comparison to the uncoated glass and the tinted glass with the same VIS transparency, meta-glass reduces the floor temperature by 12.7 and 8.3 °C, respectively. Due to its submicrometer structure, relatively simple fabrication process, and outstanding properties, the designed meta-glass holds significant potential for direct substitution of traditional glass as energy-efficient windows. Additionally, we showcase the customization results of the meta-glass with adjusted transparency of 85, 80, 70 and 60% under the same framework of DRL to meet the specific requirements of diverse usage scenarios. The presented DRL framework demonstrates powerful capabilities of material selection and structural optimization simultaneously, such as the implementation of meta-glass, offering an extensible, customized, and easy-to-implement feasible approach for designing other complex metamaterials.

RESULTS AND DISCUSSION

Design and Optimization of Meta-glass via DRL. Contrary to the supervised or unsupervised deep learning where neural networks are trained to establish mapping relationships of precollected data, neural networks in DRL are programmed to continuously interact with the environment as agents, taking actions to dynamically update the environment's state in pursuit of maximizing the reward. Here, we adopt the value-based deep Q-Network (DQN)[36] to establish the DRL framework to design and optimize the meta-glass (Figure 1d). The specific process is as follows.

1. Construction of the environment. The environment of the DRL framework represents the entire optimization process, with the state of the environment characterized by the structural parameters of DM metamaterials. Here, the DM is set as a five-layer structure composed of two alternating materials with overall consideration of spectral modulation performance, fabrication feasibility and economic viability, which can be further adjusted to suit various applications. The candidate materials encompass six dielectrics with near-zero extinction coefficients in the solar band, ensuring no absorption of solar radiation (Figure S1). Each layer thickness varies from 20 to 300 nm, with a 10 nm as interval. Consequently, above structural configuration yields a total optimization space of $6 \times 5 \times 29^5 = 6.15 \times 10^8$. The huge optimization space necessitates substantial computational resources for gradient-based and evolution-based algorithms, such as Bayesian optimization, needle optimization and genetic algorithms.[37,38] The structural parameters of DM, including two types of materials and five thicknesses, are randomly initialized for the subsequent steps.
2. Construction of the neural network. After the structural parameters of the DM is mathematically encoded, a four-layer fully connected neural network is constructed as the agent to receive the state information on the environment. The neural network is tasked with predicting the Q-value function, which represents the long-term cumulative reward for each action at a given state. Subsequently, the network outputs an action with the maximum Q-value to update the current state s_t to next state s_{t+1}. Each action corresponds a specific policy, such as replacing the materials of a specific layer or adjusting the layer thickness (more details see Supporting Information Note 2).
3. Simulation and feedback. Upon the state is updated, the transfer matrix method (TMM) is utilized to physically simulate the new structure. Following the simulation, the state is evaluated using a reward function based on calculated spectrum. The calculated reward value is then fed back to the neural network to update the true Q-value, and s_{t+1} acts as the input for the subsequent interaction. The mean square error between the true Q-value and predicted one from the neural network is adopted as the loss function to facilitate backpropagation for updating the neural network parameters, as follows.

$$loss = MSE(Q_t - Q_p) \tag{1}$$

Hence, precise definition of the reward function is crucial as it directly steers the optimization trajectory for meta-glass performance. Since DMs do not exhibit strong reflection in the MIR, they do not significantly affect the MIR emission performance when deposited on the glass substrate[31] (Figure S1). Therefore, the reward function is tailored exclusively to the solar band. To strike an equilibrium between the cooling performance and VIS transparency of meta-glass, the reward function is defined as follows:

$$reward = \alpha_1 \times (\overline{T}_{VIS} - \overline{T}_{NIR}) + \alpha_2 \times [1 - (\overline{T}_{VIS\_tar} - \overline{T}_{VIS})] \tag{2}$$

https://doi.org/10.1021/acsphotonics.4c00981
ACS Photonics XXXX, XXX, XXX−XXX

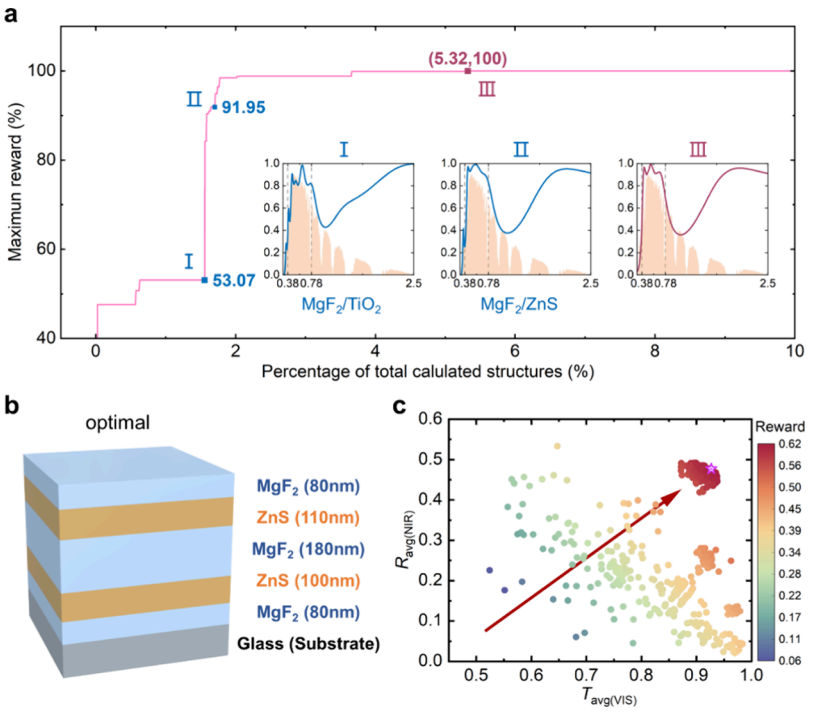

Figure 2. Optimization results of DM coating for meta-glass by the DRL framework. (a) Evolution of the maximum reward with percentage of total calculated structures. Inset: transmittance spectra of two intermediate and optimal structures during the optimization process. (b) Schematic of optimal meta-glass. (c) Average VIS transmittance and average NIR reflectance of all calculated structures during optimization. Color bar donates the reward value. Optimal structure is marked by a magenta star.

where $\overline{T}_{VIS}$ and $\overline{T}_{NIR}$ are the average AM1.5-weighted transmittances for the VIS and NIR bands, respectively (Supporting Information Note 1). $\overline{T}_{VIS\_tar} = 1$ is the target transmittance in the VIS wavelengths. α_1 and α_2 are the weights of the two terms with $\alpha_1 + \alpha_2 = 1$. The former term in eq 2 aims to maximize the difference between VIS and NIR transmittance, while the latter ensures the sufficiently high VIS transmittance. Here, α_1 and α_2 are set to 0.6 and 0.4 after numerical trials, respectively, in order to achieve VIS transparency that is comparable to common glass while achieving the optimal cooling performance.

Additionally, Experience Replay is employed to store each pair of state, action and corresponding reward, creating a data set for training the neural network, so as to predict the Q-value function more accurately over numerous iterations. The Epsilon Greedy Exploration strategy is employed to balance exploration and exploitation by initially choosing random actions with probability ε_e to facilitate the discovery of new actions, and later selecting the action with the highest Q-value function as the neural network is gradually trained. In general, DQN bolsters training stability and efficiency through iteratively taking actions, evaluating rewards, updating the Q-value function, and leveraging Experience Replay. These allow DQN to acquire the appropriate policies in a complex environment, making it particularly suitable for such extensive optimization space problems involving material selection and structural optimization simultaneously.

With the aid of the constructed DRL framework, DM metamaterials can be efficiently optimized by continuously updating the structure to maximize the reward value. Figure 2a depicts the evolution of the maximum reward as a function of the percentage of the total calculated structures. Evidently, the reward value exhibits a swift ascent, only requiring calculation of less than 2% of the structures to attain a configuration yielding 91.95% of the maximum reward. When calculating 5.23% of the structures, the reward coverages to the optimal value of 0.613, corresponding to a $\overline{T}_{VIS}$ of 92.7% and a $\overline{T}_{NIR}$ of 52% Since the DM metamaterial exhibits near-zero absorption in the NIR, the $\overline{R}_{NIR}$ of 48% can be obtained from $R = 1 - T$. The simulated solar band spectra of two intermediate structures and the optimal structure offer a clear and intuitive evolution process of the optimization (Figure 2a, inset). The VIS transmittance gradually increases while the NIR transmittance gradually decreases. Additionally, materials and structures are accurately screened and optimized by DQN. The optimal DM metamaterial comprises three layers of MgF_2 and two layers of ZnS, exhibiting nearly symmetry in the layer thicknesses (Figure 2b). With a total thickness of 550 nm on a submicrometer, the structure proves good fabrication and economic feasibility, which much outperforms the manually designed distribution Bragg reflectors (DBRs) in terms of both spectral performance and structure. (Figure S2). The performance of all calculated structures during the optimization process is depicted in Figure 2c as a scatter plot with the color bar donating the reward value, showcasing the trend of the optimization toward ultrahigh VIS transparency (>90%) and considerable NIR reflectance (~50%). The DRL framework underscores the effectiveness of the optimal design by simultaneously considering material selection and structural optimization efficiently and accurately.

Optical and IR Properties of Meta-Glass. According to the parameters of the optimal structure, we precisely deposited the MgF_2 and ZnS multilayer on a soda-lime glass substrate using electron-beam evaporation, and their thicknesses are calibrated using spectroscopic ellipsometry. The corresponding scanning electron microscope (SEM) image of the fabricated meta-glass confirms the accuracy of the fabrication, and the thickness of each layer is approximately consistent with the

https://doi.org/10.1021/acsphotonics.4c00981
ACS Photonics XXXX, XXX, XXX−XXX

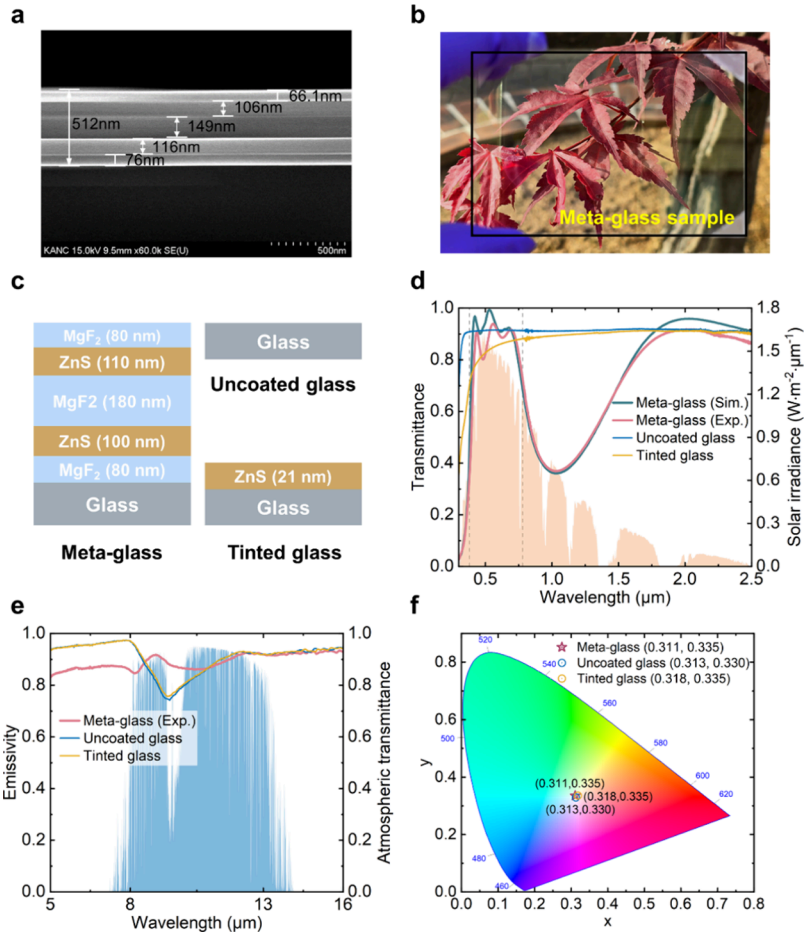

Figure 3. Optical and infrared performance of the optimal meta-glass. (a) SEM image of fabricated meta-glass. (b) Real image of fabricated meta-glass. (c) Schematic of three fabricated samples, including optimal meta-glass, uncoated glass and tinted glass with the same VIS transmittance. (d) Transmittance spectra of meta-glass (simulation and experiment), uncoated glass, and tinted glass. (e) Emissivity spectra of meta-glass, uncoated glass, and tinted glass. (f) Simulated color of three fabricated samples in CIE 1931 color space.

optimized values, with the error falling with an acceptable range (Figure 3a,c). The fabricated meta-glass sample appears nearly indistinguishable from uncoated common glass to the naked eye in outdoor environment due to its ultrahigh VIS transparency (Figure 3b). The corresponding measured transmittance spectra in the solar band match well with the simulated spectra, with a marginal reduction in the VIS, where the $\overline{T}_{VIS}$ decreases from 92.7 to 86% at normal incident (Figure 3d). This can be mainly attributed to the associated variations in the thickness-dependent optical properties of the materials. Note that we utilize numerical values at normal incident rather than the averaged over a specific angle ranges to facilitate comparison with other related works, although our meta-glass exhibits angle-independent over a wide range of angles, which will be elaborated specifically later. Unfortunately, the decrease in transmittance is only observed within the 0.78−1.5 μm (region A) but not in other NIR wavelengths (region B). Nevertheless, this does not significantly affect the cooling performance of our meta-glass, as the proportion of solar radiant energy in region A (33.3%) is much higher than that in region B (9.5%) (Figure S3), thereby emphasizing the crucial role of effective reflectance in region A in enhancing cooling performance.

To elucidate the impact of NIR reflectance, we designed and fabricated a tinted glass by depositing a single ZnS layer onto the glass substrate (Figure 3c). The layer thickness of ZnS is precisely adjusted to maintain a nearly identical VIS transparency to the fabricated meta-glass, which stood at 0.84. Furthermore, the uncoated glass with $\overline{T}_{VIS}$ of 91% also serves as a control group for performance evaluation and, akin to the tinted glass, does not exhibit substantial reflection in NIR regions (Figure 3d). The MIR emissivity spectra of the three samples were measured. The uncoated glass and tinted glass both exhibit high emission in the AW due to the strong phonon polariton resonance of silica in glass, with average emissivities of 86 and 87%, respectively (Figure 3e). The coated DM does not only significantly affect the MIR emissivity because of high IR transparency but also induce slight IR resonance, leading to a slight increase in the measured MIR emissivity of meta-glass to 89% (Figure S4). Consistent with previous related works, we also spin-coated an 80 μm PDMS atop the meta-glass to further enhance IR emission (Figure S5), as the thickness is the minimum required for high MIR emission (Figure S6). However, the relatively thick PDMS results in a blue-shift of the transmittance spectrum, significantly impacting the performance, leading to serious reductions in both $\overline{T}_{VIS}$ (80%) and $\overline{R}_{NIR}$ (40%), although the emissivity in AW increases to 0.93. Such a negative effect of PDMS on VIS and NIR bands can be also found in the previous literature.[22,23,30] However, polymers like PDMS are indispensable for them (DMD or ITO-based structures) to ensure high MIR emission to achieve TRC. Our meta-glass circumvents this reliance, thus achieving ultrahigh

https://doi.org/10.1021/acsphotonics.4c00981
ACS Photonics XXXX, XXX, XXX−XXX

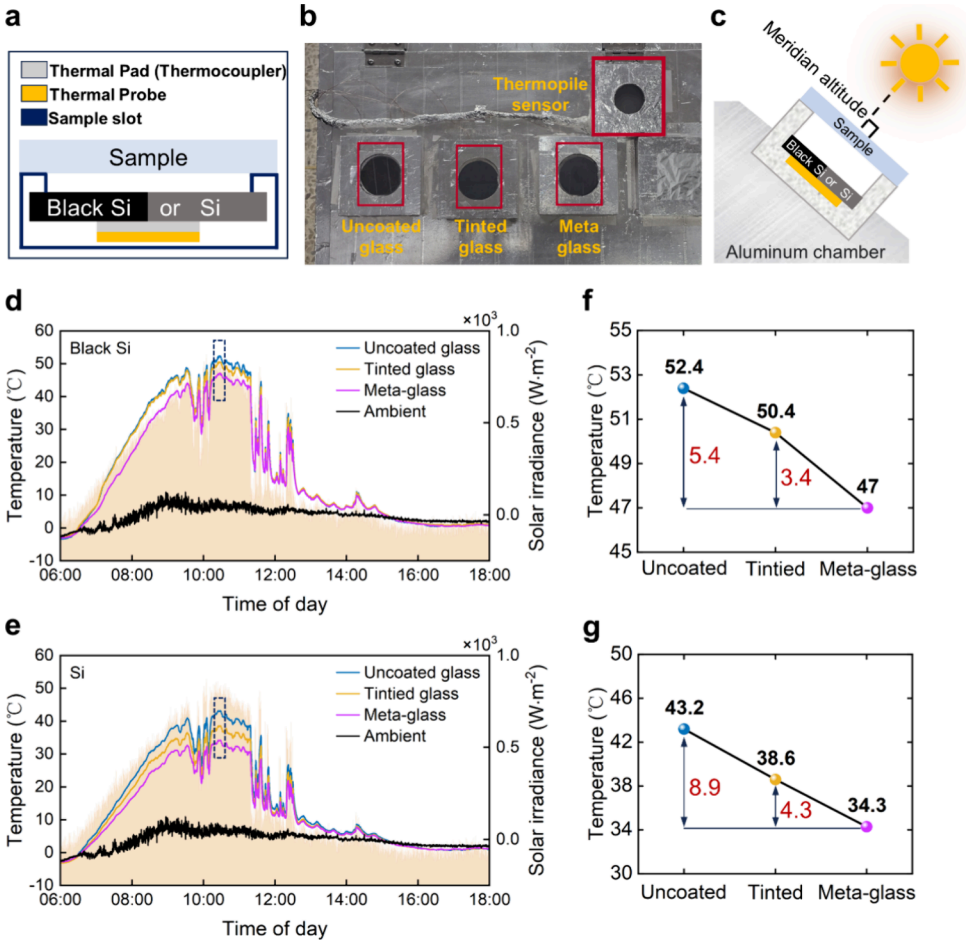

Figure 4. Field test on cooling performance of the designed meta-glass. (a) Schematic of the experimental setup simulating a thermal insulating environment with the samples as windows sealed on the top side. (b) Image of the experimental setup. Thermal insulating chambers are placed in parallel. (c) Schematic of the orientation of the experimental setup. (d) Measured floor (black Si) temperature of the three chambers as a function of time performed at Kyung Hee University, Suwon, Korea, from 6:00 to 18:00 on December 28, 2023. The ambient temperature and solar irradiance were also recorded. (e) Measured floor (Si) temperature of the three chambers as a function of time. (f) Highest floor (Black Si) temperatures of the three chambers at 10:30. (g) Highest floor (Si) temperatures of the three chambers at 10:30.

VIS transparency as well as the submicrometer structure of DM for the economics of fabrication.

Based on the CIE1931 color space, we utilized the measured data of three samples to simulate the color appearance (details see the Supporting Information, Note 3). The color difference between the meta-glass and the uncoated glass is minimal numerically (Figure 3f), and the simulated colors closely match the real images (Figure S7).

Daytime Outdoor Temperature Measurement. To estimate the practical cooling performance of the meta-glass, we examined the fabricated sample in an outdoor experiment through a thermal insulating chamber with the sample sealed on the top side. A carbon black Silicon (Si) or Si substrate, each with different solar absorptivity, was placed at the bottom of the insulation chamber to emulate different kinds of floors or interior decoration. A thermocouple was bonded to the bottom of Si, and the real-time temperature of Si rather than the inner ambient temperature was monitored due to the significant thermal resistance of the air within the chamber (Figure 4a). Additionally, another two chambers of the same configuration were arranged in parallel, except that the top is mounted with uncoated glass and tinted glass for comparison (Figure 4b). Furthermore, the entire setup is tilted at meridian altitude to ensure that solar radiation is vertically incident at noon (Figure 4c). Since the initial temperature of each chamber is the same and the difference in thermal conductivity of each sample can be negligible, the difference in temperature within the chamber can be considered to be caused by the differences in optical and radiation properties of the sample.[24,29,30] Consequently, the cooling performance of meta-glass can be intuitively demonstrated by the floor temperature differences of these chambers. The device is tested for 12 h in Suwon, South Korea (Figure 4d,e). When black Si with higher absorptivity (~90%) is utilized as the floor material, the temperature difference peaks at 10:30, and the chamber with meta-glass achieves temperature drops by 5.4 and 3.4 °C compared with chambers installed using uncoated glass and tinted glass, respectively (Figure 4f). Similarly, when employing Si with a lower absorptivity (~30%) as the floor, the meta-glass sample exhibited temperature drops of 8.9 and 4.3 °C compared with uncoated and tinted samples, respectively (Figure 4g). These results suggest that the developed meta-glass can exhibit substantial cooling effects in various floor scenarios. It is noteworthy that meta-glass exhibits such exceptional cooling effectiveness in a test environment with a maximum ambient temperature of ~10 °C together with a maximum solar radiation irradiance of 780 W/m^2. This suggests that a more evident cooling effect of meta-glass can be reasonably predicted in conditions with higher

https://doi.org/10.1021/acsphotonics.4c00981
ACS Photonics XXXX, XXX, XXX−XXX

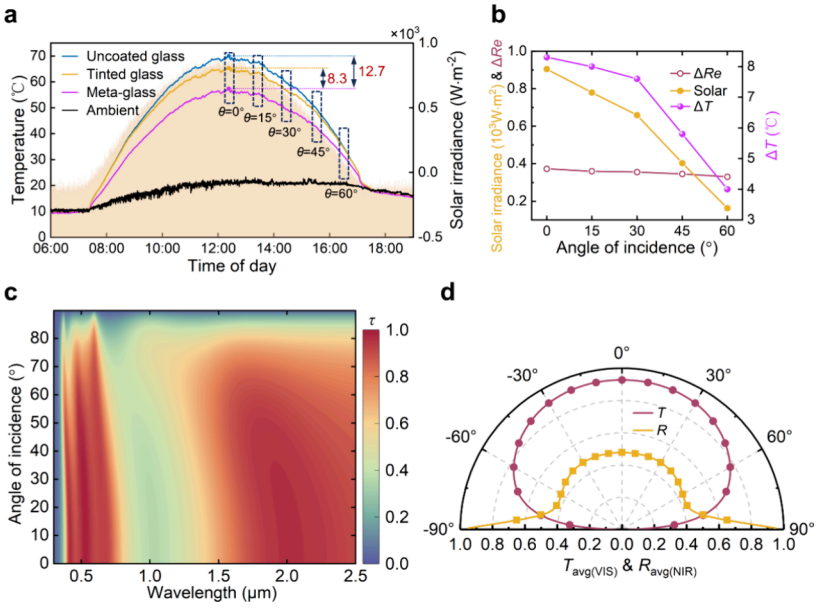

Figure 5. Field test on cooling performance of designed meta-glass, considering angular independence. (a) Measured floor (Black Si) temperatures of the three chambers as a function of time performed at Kyung Hee University, Suwon, Korea, from 6:00 to 19:00 on October 29, 2023. At different times, the solar enters at different angles of incidence, including normal, 15, 30, 45, and 60°. (b) NIR reflectance difference and floor temperature difference between meta-glass and tinted glass, and solar irradiance as a function of angle of incidence. (c) Transmittance spectrum of meta-glass as a function of wavelength and angle of incidence. (d) Average VIS transmittance and average NIR reflectance of meta-glass as a function of incident angle.

temperatures and solar radiation intensity on hot days, indicating significant potential for energy conservation.

On a clear and warmer day, we conducted another outdoor experiment to compare the performance of meta-glass with the PDMS coated meta-glass (PDMS-meta-glass) and to assess the angular correlation. The chamber with meta-glass exhibits a temperature up to 12.7 °C lower than that with uncoated glass but 2.8 °C higher than that with PDMS-meta-glass (Figure 5a, Figure S8). This can be mainly attributed to a kind of competing between the VIS transparency and cooling performance, as the micrometer scale PDMS significantly reduce the VIS transparency of meta-glass, resulting in the reduction of the average transmittance in the whole solar band (Figure S5), which in turn is conducive to block the solar energy. Nevertheless, we reiterate that VIS transparency is more important than cooling performance, as it determines the feasibility of meta-glass for directly applied as energy-saving windows in general scenarios. In situations where high transparency is not a crucial requirement, customized meta-glass can be employed to enhance cooling effects without the need for an additional polymer layer, which will be discussed later. To present the impact of solar incidence angles on cooling performance, we approximated solar radiation over time to represent various solar incidence angles. We focus on the contrast between the meta-glass and tinted glass due to their consistent VIS transparency. Figure 5b illustrates the variation of performance with the solar incidence angles, where ΔRe represents the NIR reflectance difference (red line), ΔT represents the temperature difference (magenta line), and yellow line represents the solar irradiance. As the incidence angle increases, ΔRe remains almost constant while the ΔT gradually decreases. Hence, the decrease in ΔT is attributed to the reduced solar irradiance. Nevertheless, meta-glass still maintains a ΔT of 4 to 8.3 °C across various incident angles, which attributes to considerable and angle-independent NIR reflection of meta-glass, especially in region A when compared with the tinted sample. To make a clear exhibition of angle independence, simulation results indicate that the $\overline{T}_{VIS}$ of meta-glass remains consistently high level up to angles of less than 60°, and $\overline{R}_{NIR}$ even remains stable at angles of below 70° (Figure 5c,d). The abrupt increase in reflectance beyond 70° can be attributed to the total reflection effect of light. This excellent angle-independence ensures that the meta-glass installed vertically on buildings exhibits stable cooling performance.[39,40] On the contrary, the $\overline{R}_{NIR}$ of PDMS-meta-glass exhibits significant angular dependence, decreasing as the angle increases (Figure S9). This impact of PDMS on the angular independence of the solar transmission (reflection) has been seldom discussed in previous studies (Figure S10).

Customization of Meta-Glass with Varying Transparency. Considering that we have attained a meta-glass with ultrahigh VIS transparency, providing nearly the same visual appearance as uncoated glass, and exhibiting outstanding passive cooling performance, it is still worth exploring whether the customized meta-glass with discrete levels of VIS transparency can be designed so that their NIR reflectance and radiative cooling performance can be enhanced. Such customized meta-glass could find applications in settings with no specific requirement for high VIS transparency, such as building sunroofs or automobile skylight. Thus, we present tailored outcomes for meta-glasses with diverse VIS transparency, utilizing the advanced metamaterials design capabilities of the DRL framework.

During the design process, the reward function (eq 2) must be adjusted to satisfy the customized spectral objective, with α_1 and α_2 set to 0.4 and 0.6, respectively, to prioritize achieving the target VIS transparency $\overline{T}_{VIS\_tar}$. When targeting a VIS transparency of 85%, the $\overline{R}_{NIR}$ of meta-glass is notably enhanced, particularly in the region A of the NIR (Figure 6a). For $\overline{T}_{VIS\_tar}$ of 80, 70, and 60%, we also successfully optimize the structures to meet the corresponding objective, and the $\overline{R}_{NIR}$ of which all surpasses that of the meta-glass with optimal $\overline{T}_{VIS}$. Detailed numerical comparisons are outlined in Table 1. The customized

https://doi.org/10.1021/acsphotonics.4c00981
ACS Photonics XXXX, XXX, XXX−XXX

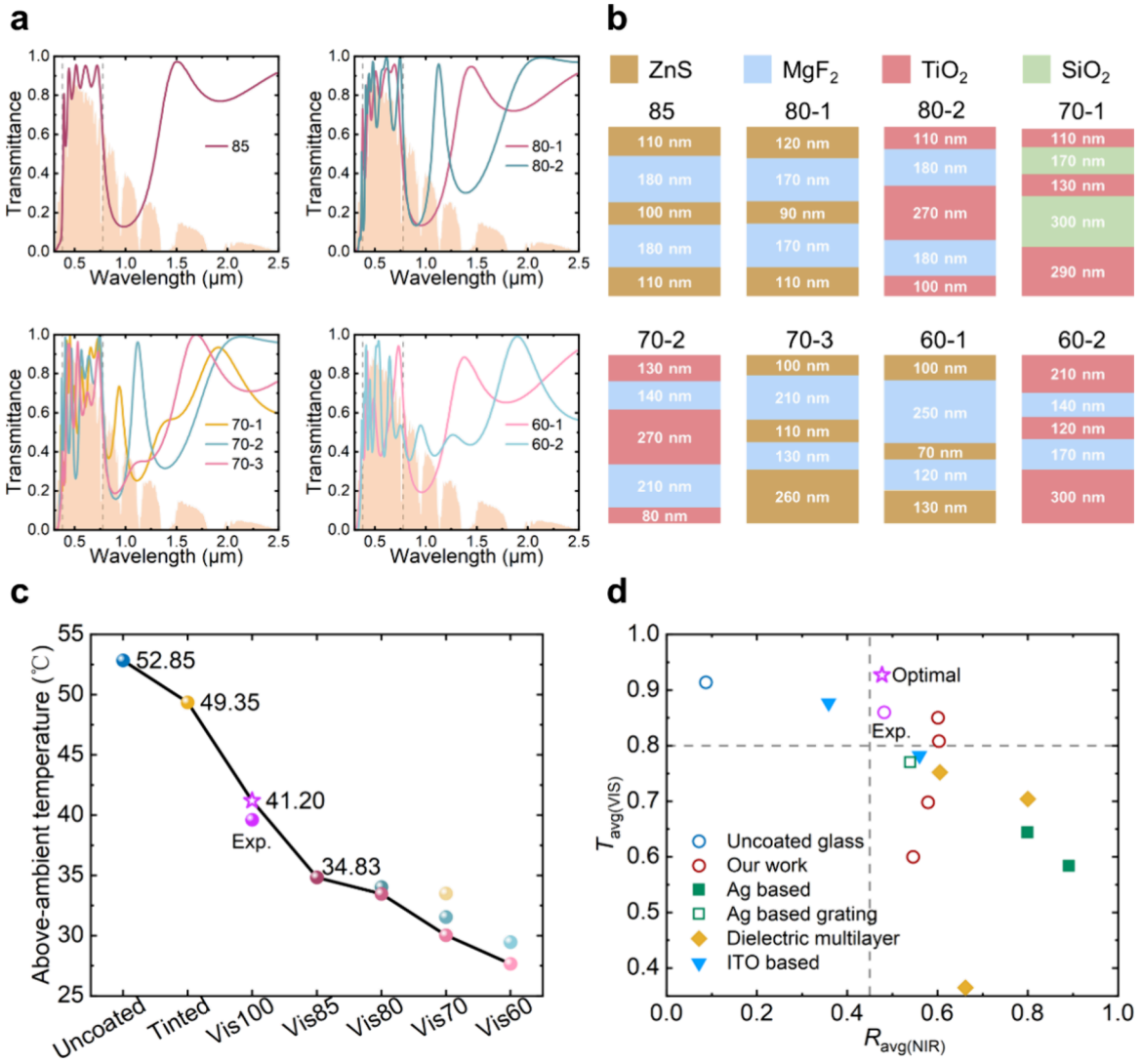

Figure 6. Customization of meta-glasses with discrete levels of VIS transparency and comparison with related works. (a) Customized transmittance spectra of meta-glasses by the DRL framework, targeting VIS transparencies of 0.85, 0.8, 0.7, and 0.6, respectively. (b) Corresponding schematic of meta-glasses with different transparencies. The same target transparency can be achieved through different structures. (c) Simulated steady-state temperature (difference from ambient temperature) for meta-glasses with different transparencies. (d) Comparison of the average VIS transmittance and average NIR reflectance between our designed meta-glasses and other related works. These works are classified according to the solar reflection techniques.

Table 1. VIS and NIR Performance and Color Appearance of Customized Meta-Glass

Meta-glass (Named by target VIS transparency)	$\bar{T}_{VIS}$	$\bar{R}_{NIR}$	Color (Simulation)
100 (Optimal Exp.)	86%	48%	
85	85%	60%	
80-1	81%	60%	
80-2	80%	57%	
70-1	74%	51%	
70-2	71%	55%	
70-3	70%	58%	
60-1	60%	55%	
60-2	63%	52%	

meta-glasses display diverse colors; particularly, when the VIS transparency is reduced, the nonuniformity of their VIS transmittance leads to more vivid colors as shown in Table 1. It should be noted that the simulated colors only demonstrate their appearance in the CIE1931 color space and do not reflect their visual transparency performance. An intriguing aspect is that meta-glass, possessing a defined color and VIS transparency, can be personalized by incorporating a color term into the

https://doi.org/10.1021/acsphotonics.4c00981
ACS Photonics XXXX, XXX, XXX−XXX

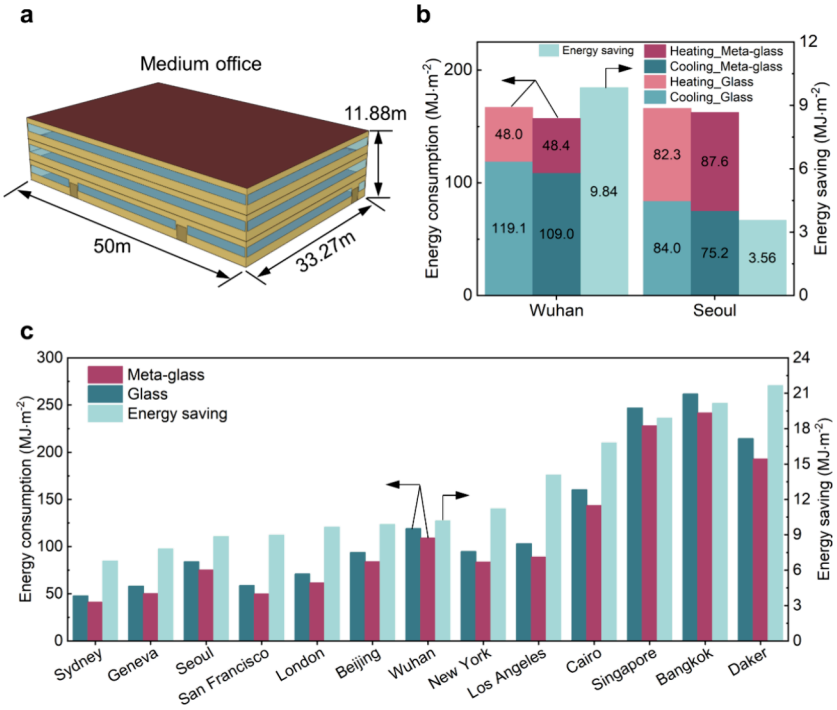

Figure 7. Evaluation of energy conservation potential. (a) Medium office model applying meta-glass as window glass material. (b) Calculated annual energy consumption for heating and cooling as well as energy saving in Wuhan and Seoul. (c) Calculated annual energy consumption and energy saving data in typical cities of different climatic zones. Uncoated common glass serves as the comparison group.

reward function, thus expanding the potential applications of meta-glass. Moreover, leveraging the material selection capability of DQN facilitates the exploration of diverse materials to achieve the same transparency goal, thereby offering manufacturers a wider range of solutions to meet specific process and material needs (Figure 6b, Table 1). Regrettably, we fail to observe a significant enhancement of NIR reflectance at the expense of VIS transparency, primarily due to the absence of high refractive index candidate materials resulting in insufficient band gap width of photonic structure, such as Si, etc. However, introducing Si could result in solar absorption by the meta-glass because of nonzero extinction coefficient, leading to a trade-off between performance and customization. We conducted theoretical calculations on the cooling effect of meta-glasses with discrete levels of VIS transparency (calculation details see the Supporting Information, Note 4). As VIS transparency is progressively decreases, the cooling effect of meta-glass is predictably enhanced because of reduced transmission of solar energy (Figure 6c). We believe that meta-glasses with $\overline{T}_{VIS}$ values of 85 or 80% appear to be suitable choices for situations where the demand for transparency is not particularly high and enhanced cooling performance is desired.

To highlight the advantages of the DRL-optimized meta-glass, we compared all meta-glasses in our work with published TRC works, which are categorized based on solar management technology (Figure 6d). The optimal structure demonstrates a significant advantage in VIS transparency, almost consistent with uncoated glass, which we emphasize again. This advantage enables it to be a viable substitute for window materials to achieve energy conservation. With a slight reduction in VIS transparency when considering a trade-off between cooling performance and visual sense, meta-glasses with $\overline{T}_{VIS}$ values of 85 and 80% in our work still exhibit quite competitive in NIR reflection compared with other works.

Energy Conservation Potential. To evaluate the energy-saving capabilities of the meta-glass, an energy consumption simulation is conducted based on a medium office model (Figure 7a). The meta-glass with ultrahigh VIS transparency was applied as window glass material of the office, and the uncoated common glass is served as control group for comparison (for details for the simulation, see the Supporting Information, Note 5). The significant positive energy conservation effects can be observed in both Wuhan and Seoul when considering year-around energy consumption for cooling and heating, although the supercooling effect of meta-glass in cold days will lead to an increase in heating energy consumption (Figure 7b). When focusing on cooling energy consumption, considerable energy conservation effects across representative cities in different climate zones can be observed with energy savings ranging from 7 to 21 MJ/m^2 compared with common glass (Figure 7c). When considering annual cooling and heating energy consumption, meta-glass also demonstrates remarkable energy conservation potential in most climate zones (Figure S11).

CONCLUSIONS

In conclusion, we report an ultrahigh VIS transparency, submicrometer and polymer-free DM coated meta-glass optimized by the DRL framework. Guided by the target spectrum, the material selection and structural optimization are simultaneously performed autonomously and efficiently by DRL. The optical and infrared properties of designed meta-glass are experimentally demonstrated, matching well with the simulation results. Benefitting from the polymer-free structure, meta-glass exhibits excellent angle independence in the spectrum. In outdoor cooling effect measurement, the fabricated meta-glass reduces the floor temperatures by up to 12.7 and 8.3 °C at an ambient temperature of about 20 °C, in comparison to the uncoated glass and tinted glass with consistent VIS

https://doi.org/10.1021/acsphotonics.4c00981
ACS Photonics XXXX, XXX, XXX−XXX

transparency. At an ambient temperature of about 10 °C, the temperature drops can also reach 8.9 and 4.3 °C. The ultrahigh VIS transparency consistent with uncoated common glass and together with outstanding passive cooling performance make meta-glass a direct substitute for window materials to enable energy conservation in most climates. Additionally, with the aid of DRL, customization results with varying levels of VIS transparency are presented when considering sacrificing transparency to obtain greater cooling effects to meet the requirements of different application scenarios. Furthermore, the DRL framework can be feasibly utilized for metamaterial design in other fields beyond TRC.

MATERIALS AND METHODS

Simulations. The meta-glass's visible transmittance and infrared emissivity was simulated using the TMM. The refractive index and extinction coefficient of SiO_2 were referred to Palik's book.[41] The optical constants of TiO_2 were referred to ref 42. The optical constants of ZnS were referred to ref 43. The optical constants of Al_2O_3, MgF_2 and Si_3N_4 are taken from ref 44. Color simulation were performed using MATLAB with our code, the principle of which and details can be found in the Supporting Information, Note 3. The construction of DRL framework was performed using Python with the help of open-source package TensorFlow. The number of neurons in the three intermediate fully connected layers is 24, 48, and 24. The number of neurons in the input layer and output layer correspond to the structural parameters of meta-glass and the number of actions that can be taken, namely, 7 and 14, respectively.

Sample Fabrication. The MgF_2 and ZnS layers of meta-glass were alternately deposited on the soda-lime glass substrate using an electron beam evaporator (UEE, ULTEC). During deposition, the deposition rate and accumulated thickness of each layer were continuously monitored using a quartz crystal monitor. To ensure the accuracy and precision in the measurements, the film thicknesses were subsequently validated using a spectroscopic ellipsometer (Elli-SE, Ellipso Technology).

Optical Characterization. The visible transmittance spectra of the fabricated meta-glass and other samples were measured using a spectrophotometer (Cary5000, Thermo Fisher). The infrared emissivity spectra of the fabricated meta-glass and other samples were measured using a Fourier transform infrared spectrometer (INVENIO R, Bruker)

Outdoor Temperature Measurement. To exclude unwanted thermal interaction, four cylindrical chambers, each 20 mm in height and 55 mm in diameter, were prepared. The sides of chambers except the top were covered with aluminum film to reflect sunlight and prevent heating. The top sides of the chambers were covered and sealed by the 76 mm × 52 mm meta-glass and other reference samples, including uncoated glass, tinted glass, and meta-glass with PDMS. Therefore, the convective heat transfer in the airtight chamber can be neglected. Then, a 2 in. piece of black Si or Si was positioned at the bottom to depict various interior decorations, with the black Si exhibiting the absorptivity of about 0.9, and the Si of 0.3. A thermal probe (SA1-K-72-SC, Omega Engineering) connected to a data logger (RDXL12SD, Omega Engineering) is attached to the bottom of black Si or Si to monitor its temperature in real-time. Therefore, the temperature variations in each chamber indicate the cooling effect of the meta-glass. Due to numerous complex factors, such as building scale, ventilation levels, and conduction/convection coefficients, measuring the inner ambient temperature within our centimeter-scale cylindrical chamber would not yield practical results, as the setup does not accurately represent a real building environment. Additionally, the solar irradiance was measured using a thermopile sensor (919P-040−50, Newport).

ASSOCIATED CONTENT

Data Availability Statement

The data are available from the authors upon a reasonable request.

Supporting Information

The Supporting Information is available free of charge at https://pubs.acs.org/doi/10.1021/acsphotonics.4c00981.

Detailed calculation of average transmittance, reflectance and emissivity; detailed description of material selection and structural optimization by DRL framework; detailed calculation of color simulation; detailed simulation of the cooling effect of meta-glass; detailed simulation of energy conservation potential of meta-glass; additional supporting tables and figures (PDF)

AUTHOR INFORMATION

Corresponding Authors

Sun-Kyung Kim − *Department of Applied Physics, Kyung Hee University, Yongin-Si, Gyeonggi-do 17104, Republic of Korea;* orcid.org/0000-0002-0715-0066; Email: sunkim@khu.ac.kr

Run Hu − *School of Energy and Power Engineering, Huazhong University of Science and Technology, Wuhan 430074, China; Department of Applied Physics, Kyung Hee University, Yongin-Si, Gyeonggi-do 17104, Republic of Korea; Wuhan National Laboratory for Optoelectronics, Huazhong University of Science and Technology, Wuhan 430074, China;* orcid.org/0000-0003-0274-9982; Email: hurun@hust.edu.cn

Authors

Shilv Yu − *School of Energy and Power Engineering, Huazhong University of Science and Technology, Wuhan 430074, China*

Jae-Seon Yu − *Department of Applied Physics, Kyung Hee University, Yongin-Si, Gyeonggi-do 17104, Republic of Korea*

Zihe Chen − *School of Energy and Power Engineering, Huazhong University of Science and Technology, Wuhan 430074, China*

Qinghe Li − *School of Energy and Power Engineering, Huazhong University of Science and Technology, Wuhan 430074, China*

Zhaochen Wang − *School of Energy and Power Engineering, Huazhong University of Science and Technology, Wuhan 430074, China*

Xiaobing Luo − *School of Energy and Power Engineering, Huazhong University of Science and Technology, Wuhan 430074, China;* orcid.org/0000-0002-6423-9868

Complete contact information is available at: https://pubs.acs.org/10.1021/acsphotonics.4c00981

Author Contributions

#S.Y. and J.-S.Y. contributed equally.

Notes

The authors declare no competing financial interest.

https://doi.org/10.1021/acsphotonics.4c00981
ACS Photonics XXXX, XXX, XXX−XXX

■ ACKNOWLEDGMENTS

R.H. would like to acknowledge the financial support by the National Natural Science Foundation of China (52211540005, 52076087), Science and Technology Program of Hubei Province (2023AFA072), the Open Project Program of Wuhan National Laboratory for Optoelectronics (2021WNLOKF004), and Wuhan Knowledge Innovation Shuguang Program. S.-Y.K. acknowledgements the support by the National Research Foundation of Korea (NRF) through the Basic Science Research Program (RS-2023-00207966).

■ REFERENCES

(1) Liang, J.; Wu, J.; Guo, J.; Li, H.; Zhou, X.; Liang, S.; Qiu, C. W.; Tao, G. Radiative Cooling for Passive Thermal Management towards Sustainable Carbon Neutrality. *Natl. Sci. Rev.* **2023**, *10* (1), No. nwac208.

(2) Ürge-Vorsatz, D.; Cabeza, L. F.; Serrano, S.; Barreneche, C.; Petrichenko, K. Heating and Cooling Energy Trends and Drivers in Buildings. *Renew. Sust. Energy Rev.* **2015**, *41*, 85−98.

(3) Grynning, S.; Gustavsen, A.; Time, B.; Jelle, B. P. Windows in the Buildings of Tomorrow: Energy Losers or Energy Gainers? *Energy Buildings* **2013**, *61*, 185−192.

(4) Hee, W. J.; Alghoul, M. A.; Bakhtyar, B.; Elayeb, O.; Shameri, M. A.; Alrubaih, M. S.; Sopian, K. The Role of Window Glazing on Daylighting and Energy Saving in Buildings. *Renew. Sust. Energy Rev.* **2015**, *42*, 323−343.

(5) Fan, S.; Li, W. Photonics and Thermodynamics Concepts in Radiative Cooling. *Nat. Photonics* **2022**, *16*, 182−190.

(6) Zhou, L.; Song, H.; Liang, J.; Singer, M.; Zhou, M.; Stegenburgs, E.; Zhang, N.; Xu, C.; Ng, T.; Yu, Z.; Ooi, B.; Gan, Q. A Polydimethylsiloxane-Coated Metal Structure for All-Day Radiative Cooling. *Nat. Sustain.* **2019**, *2* (8), 718−724.

(7) Cho, J.-W.; Lee, E.-J.; Kim, S.-K. Radiative Cooling Technologies: A Platform for Passive Heat Dissipation. *J. Korean Phys. Soc.* **2022**, *81* (6), 481−489.

(8) Lin, K.; Chen, S.; Zeng, Y.; Ho, T. C.; Zhu, Y.; Wang, X.; Liu, F.; Huang, B.; Chao, C. Y.-H.; Wang, Z.; Tso, C. Y. Hierarchically Structured Passive Radiative Cooling Ceramic with High Solar Reflectivity. *Science* **2023**, *382* (6671), 691−697.

(9) Yin, X.; Yang, R.; Tan, G.; Fan, S. Terrestrial Radiative Cooling: Using the Cold Universe as a Renewable and Sustainable Energy Source. *Science* **2020**, *370* (6518), 786−791.

(10) Zhai, Y.; Ma, Y.; David, S. N.; Zhao, D.; Lou, R.; Tan, G.; Yang, R.; Yin, X. Scalable-Manufactured Randomized Glass-Polymer Hybrid Metamaterial for Daytime Radiative Cooling. *Science* **2017**, *355* (6329), 1062−1066.

(11) Zhou, J.; Chen, T. G.; Tsurimaki, Y.; Hajj-Ahmad, A.; Fan, L.; Peng, Y.; Xu, R.; Wu, Y.; Assawaworrarit, S.; Fan, S.; Cutkosky, M. R.; Cui, Y. Angle-Selective Thermal Emitter for Directional Radiative Cooling and Heating. *Joule* **2023**, *7*, 2830.

(12) Mandal, J.; Fu, Y.; Overvig, A. C.; Jia, M.; Sun, K.; Shi, N. N.; Zhou, H.; Xiao, X.; Yu, N.; Yang, Y. Hierarchically Porous Polymer Coatings for Highly Efficient Passive Daytime Radiative Cooling. *Science* **2018**, *362* (6412), 315−319.

(13) Tang, K.; Dong, K.; Li, J.; Gordon, M. P.; Reichertz, F. G.; Kim, H.; Rho, Y.; Wang, Q.; Lin, C.-Y.; Grigoropoulos, C. P.; Javey, A.; Urban, J. J.; Yao, J.; Levinson, R.; Wu, J. Temperature-Adaptive Radiative Coating for All-Season Household Thermal Regulation. *Science* **2021**, *374* (6574), 1504−1509.

(14) Heo, S. Y.; Lee, G. J.; Kim, D. H.; Kim, Y. J.; Ishii, S.; Kim, M. S.; Seok, T. J.; Lee, B. J.; Lee, H.; Song, Y. M. A Janus Emitter for Passive Heat Release from Enclosures. *Sci. Adv.* **2020**, *6* (36), No. eabb1906.

(15) Wang, S.; Jiang, T.; Meng, Y.; Yang, R.; Tan, G.; Long, Y. Scalable Thermochromic Smart Windows with Passive Radiative Cooling Regulation. *Science* **2021**, *374* (6574), 1501−1504.

(16) Li, J.; Liang, Y.; Li, W.; Xu, N.; Zhu, B.; Wu, Z.; Wang, X.; Fan, S.; Wang, M.; Zhu, J. Protecting Ice from Melting under Sunlight via Radiative Cooling. *Sci. Adv.* **2022**, *8* (6), No. eabj9756.

(17) Zhang, Q.; Wang, S.; Wang, X.; Jiang, Y.; Li, J.; Xu, W.; Zhu, B.; Zhu, J. Recent Progress in Daytime Radiative Cooling: Advanced Material Designs and Applications. *Small Methods* **2022**, *6* (4), No. 2101379.

(18) Yi, Z.; Lv, Y.; Xu, D.; Xu, J.; Qian, H.; Zhao, D.; Yang, R. Energy Saving Analysis of a Transparent Radiative Cooling Film for Buildings with Roof Glazing. *Energy Built Environ.* **2021**, *2* (2), 214−222.

(19) Gamage, S.; Kang, E. S. H.; Åkerlind, C.; Sardar, S.; Edberg, J.; Kariis, H.; Ederth, T.; Berggren, M.; Jonsson, M. P. Transparent Nanocellulose Metamaterial Enables Controlled Optical Diffusion and Radiative Cooling. *J. Mater. Chem. C* **2020**, *8* (34), 11687−11694.

(20) Zou, H.; Wang, C.; Yu, J.; Huang, D.; Yang, R.; Wang, R. Eliminating Greenhouse Heat Stress with Transparent Radiative Cooling Film. *Cell Rep. Phys. Sci.* **2023**, *4* (8), No. 101539.

(21) Lee, K. W.; Lim, W.; Jeon, M. S.; Jang, H.; Hwang, J.; Lee, C. H.; Kim, D. R. Visibly Clear Radiative Cooling Metamaterials for Enhanced Thermal Management in Solar Cells and Windows. *Adv. Funct. Mater.* **2022**, *32* (1), No. 2105882.

(22) Jin, Y.; Jeong, Y.; Yu, K. Infrared-Reflective Transparent Hyperbolic Metamaterials for Use in Radiative Cooling Windows. *Adv. Funct. Mater.* **2023**, *33* (1), No. 2207940.

(23) Li, Y.; Chen, X.; Yu, L.; Pang, D.; Yan, H.; Chen, M. Janus Interface Engineering Boosting Visibly Transparent Radiative Cooling for Energy Saving. *ACS Appl. Mater. Interfaces* **2023**, *15* (3), 4122−4131.

(24) Dang, S.; Wang, X.; Ye, H. An Ultrathin Transparent Radiative Cooling Photonic Structure with a High NIR Reflection. *Adv. Mater. Interfaces* **2022**, *9* (30), No. 2201050.

(25) Zhang, X.; Li, X.; Wang, F.; Yuan, W.; Cheng, Z.; Liang, H.; Yan, Y. Low-Cost and Large-Scale Producible Biomimetic Radiative Cooling Glass with Multiband Radiative Regulation Performance. *Adv. Opt. Mater.* **2022**, *10* (23), No. 2202031.

(26) Zhou, Z.; Wang, X.; Ma, Y.; Hu, B.; Zhou, J. Transparent Polymer Coatings for Energy-Efficient Daytime Window Cooling. *Cell Rep. Phys. Sci.* **2020**, *1* (11), No. 100231.

(27) Park, S. H.; Oh, Y.-K.; Lim, Y.-J.; Shaozheng, C.; Lee, S.-J.; Kim, H.-K. Thermally Stable and Transparent F-Doped SnO2 (FTO) /Ag/FTO Films for Transparent Thin Film Heaters Used in Automobiles. *Ceram. Int.* **2023**, *49* (2), 2419−2426.

(28) Sun, K.; Riedel, C. A.; Wang, Y.; Urbani, A.; Simeoni, M.; Mengali, S.; Zalkovskij, M.; Bilenberg, B.; De Groot, C. H.; Muskens, O. L. Metasurface Optical Solar Reflectors Using AZO Transparent Conducting Oxides for Radiative Cooling of Spacecraft. *ACS Photonics* **2018**, *5* (2), 495−501.

(29) Kim, S.; Shang, W.; Moon, S.; Pastega, T.; Lee, E.; Luo, T. High-Performance Transparent Radiative Cooler Designed by Quantum Computing. *ACS Energy Lett.* **2022**, *7*, 4134−4141.

(30) Kim, M.; Lee, D.; Son, S.; Yang, Y.; Lee, H.; Rho, J. Visibly Transparent Radiative Cooler under Direct Sunlight. *Adv. Opt. Mater.* **2021**, *9* (13), No. 2002226.

(31) Zhu, Y.; Luo, H.; Yang, C.; Qin, B.; Ghosh, P.; Kaur, S.; Shen, W.; Qiu, M.; Belov, P.; Li, Q. Color-Preserving Passive Radiative Cooling for an Actively Temperature-Regulated Enclosure. *Light Sci. Appl.* **2022**, *11* (1), 122.

(32) Guan, Q.; Raza, A.; Mao, S. S.; Vega, L. F.; Zhang, T. Machine Learning-Enabled Inverse Design of Radiative Cooling Film with On-Demand Transmissive Color. *ACS Photonics* **2023**, *10* (3), 715−726.

(33) St-Jean, P.; Clark, O. G.; Jemtrud, M. A Review of the Effects of Architectural Stimuli on Human Psychology and Physiology. *Build. Environ.* **2022**, *219*, No. 109182.

(34) Zhao, B.; Hu, M.; Ao, X.; Chen, N.; Pei, G. Radiative Cooling: A Review of Fundamentals, Materials, Applications, and Prospects. *Appl. Energy* **2019**, *236*, 489−513.

(35) Song, J.; Shen, Q.; Shao, H.; Deng, X. Anti-Environmental Aging Passive Daytime Radiative Cooling. *Adv. Sci.* **2023**, *11* (10), No. 2305664.

https://doi.org/10.1021/acsphotonics.4c00981
ACS Photonics XXXX, XXX, XXX−XXX

(36) Mnih, V.; Kavukcuoglu, K.; Silver, D.; Rusu, A. A.; Veness, J.; Bellemare, M. G.; Graves, A.; Riedmiller, M.; Fidjeland, A. K.; Ostrovski, G.; Petersen, S.; Beattie, C.; Sadik, A.; Antonoglou, I.; King, H.; Kumaran, D.; Wierstra, D.; Legg, S.; Hassabis, D. Human-Level Control through Deep Reinforcement Learning. *Nature* **2015**, *518* (7540), 529−533.
(37) Yu, S.; Zhou, P.; Xi, W.; Chen, Z.; Deng, Y.; Luo, X.; Li, W.; Shiomi, J.; Hu, R. General Deep Learning Framework for Emissivity Engineering. *Light Sci. Appl.* **2023**, *12* (1), 291.
(38) Kim, J.-H.; Kim, D. I.; Lee, S. S.; An, K.-S.; Yim, S.; Lee, E.; Kim, S.-K. Wide-Angle Deep Ultraviolet Antireflective Multilayers via Discrete-to-Continuous Optimization. *Nanophotonics* **2023**, *12* (10), 1913−1921.
(39) Bae, M.; Kim, D. H.; Kim, S.-K.; Song, Y. M. Transparent Energy-Saving Windows Based on Broadband Directional Thermal Emission. *Nanophotonics* **2024**, *13* (5), 749−761.
(40) Kim, S.; Jung, S.; Bobbitt, A.; Lee, E.; Luo, T. Wide-Angle Spectral Filter for Energy-Saving Windows Designed by Quantum Annealing-Enhanced Active Learning. *Cell Reports Physical Science* **2024**, *5* (3), No. 101847.
(41) Palik, E. D. *Handbook of Optical Constants of Solids*; Academic Press, 1998.
(42) Siefke, T.; Kroker, S.; Pfeiffer, K.; Puffky, O.; Dietrich, K.; Franta, D.; Ohlídal, I.; Szeghalmi, A.; Kley, E.-B.; Tünnermann, A. Materials Pushing the Application Limits of Wire Grid Polarizers Further into the Deep Ultraviolet Spectral Range. *Adv. Opt. Mater.* **2016**, *4* (11), 1780−1786.
(43) Querry, M. R. *Optical Constants of Minerals and Other Materials from the Millimeter to the Ultraviolet*; Chemical Research, Development & Engineering Center, U.S. Army Armament Munitions Chemical Command, 1987.
(44) Zaman, M. A. Photonic Radiative Cooler Optimization Using Taguchi's Method. *Int. J. Therm. Sci.* **2019**, *144*, 21−26.

https://doi.org/10.1021/acsphotonics.4c00981
ACS Photonics XXXX, XXX, XXX−XXX